It is interesting to note that polymer electrodeposition at potentials below -1.45 V is quite sensitive to the structural details of the electrode substrate. Figures 3 and 4a-c show examples of polymer deposited along step sites that are exposed on the otherwise atomically smooth basal plane of HOPG. These results demonstrate that defects provide a significantly larger number of sites conducive to polymer nucleation leading to stable polymer deposits. Consequently, STM images of the $[Re(CO)_3(vbpy)Cl]$-based polymers reflect not only the molecular details of the polymer but also the structure of the underlying substrate. For example, the polymer strand in Figure 3 follows the contour of an 8 Å high step. In this instance, multiple points of attachment must occur, since the structural correlation between the step and the polymer extends over a distance of 3000 Å. We point out that preferential nucleation at step sites on HOPG is not always observed. For example, polymer is clearly absent from the step site observed at the bottom of Figure 3b.

As a final note, the ability to image large polymeric structures, such as the 200-300 Å spherical aggregates shown in Figure 4, requires comment since direct tunneling between the STM tip and the HOPG surface over such a distance is unreasonable. We speculate that electron conduction within the interior of the polymer is supported by diffusional or migrational electron transport via a redox conduction mechanism.[19] Dry films of partially oxidized or reduced redox polymers, e.g., poly(vinylferrocene)$^{0/+}$, when sandwiched between two macroscopic metal contacts (i.e., metal/polymer/metal) conduct electrons at a rate controlled by electron hopping between oxidized and reduced sites.[20,21] These solid-state polymer-based electrochemical cells, in fact, closely resemble the Pt-Rh tip/polymer/HOPG structure that is engaged in STM imaging of the electrodeposited $[Re(CO)_3(vbpy)Cl]$-based polymer.

(19) Murray, R. W. *Electroanalytical Chemistry*; Bard, A. J., Ed.; Wiley: New York, 1984; Vol. 14, and references therein.
(20) Jerigan, J. C.; Chidsey, C. E. D.; Murray, R. W. *J. Am. Chem. Soc.* **1985**, *107*, 2824.
(21) Hagemeister, M. P.; White, H. S. *J. Phys. Chem.* **1987**, *91*, 150.

Conclusions

STM results reported here demonstrate that the chemical composition and structure of $[Re(CO)_3(vbpy)Cl]$-based films are remarkably dependent on conditions employed in electrodeposition. Polymeric materials with several different morphologies are observed when the deposition is carried out to -1.45 V vs SSCE. A more uniform surface coverage of discrete molecules is observed when the potential is scanned to -2.0 V to promote the formation of the Re-Re dimers. On the basis of the size and shape of these entities, we tentatively assign them as products derived from vinyl-vinyl coupling of Re-Re bonded dimers: $[(vbpy)(CO)_3Re\text{-}Re(CO)_3(vbpyH\text{-}vbpyH)(CO)_3Re\text{-}Re(CO)_3(vbpy)]$.

The ability to resolve individual molecules as well as the molecular subunits in the $[Re(CO)_3(vbpy)Cl]$-based polymer suggest that STM studies may be valuable in identifying the structure of surface-adsorbed organometallic species. In addition, the substitutional chemistry of $[Re(CO)_3(vbpy)Cl]$ and other similar metal complexes containing polymerizable ligands is significant thus broadening the range of applications. We are currently exploring these and other areas.

Acknowledgment. STM facilitates are supported by the Center for Interfacial Engineering with funding from NSF Engineering Research Centers Program (CDR 8721551) and industrial sponsors. Work at the University of Minnesota is supported by the Office of Naval Research Young Investigator Program. Work at Cornell was supported in part by the National Science Foundation. S.L. acknowledges support by a MARC Fellowship from the NIH. H.D.A. is the recipient of a Presidential Young Investigator Award (1984-1989) and an A. P. Sloan Fellowship (1987-1991).

Electrochemistry of NADH/NAD$^+$ Analogues. A Detailed Mechanistic Kinetic and Thermodynamic Analysis of the 10-Methylacridan/10-Methylacridinium Couple in Acetonitrile

Philippe Hapiot,[1a] Jacques Moiroux,[1b] and Jean-Michel Savéant*.[1a]

Contribution from the Laboratoire d'Electrochimie Moléculaire de l'Université de Paris 7, Unité de Recherche Associée au CNRS No. 438, 2, Place Jussieu, 75231 Paris Cedex 05, France, and the Laboratoire de Chimie Analytique, Université de Paris 5, Unité de Recherche Associée No. 484, 4, Avenue de l'Observatoire, 75270 Paris Cedex 05, France. *Received July 7, 1989*

Abstract: The electrochemical oxidation of 10-methylacridan (AH) at platinum and gold electrodes in acetonitrile containing various pyridine bases is investigated by means of cyclic voltammetric and potential step techniques. The conversion of AH to the 10-methylacridinium ion (A^+) proceeds along an electron-proton-electron transfer mechanism, the second electron being abstracted by the initial cation radical, $AH^{\bullet+}$, rather than by the electrode itself in most cases. The use of ultramicroelectrodes (in the 10 μm diameter range) allows the determination of the standard potential of the $AH^{\bullet+}/AH$ couple and of the rate constant of the deprotonation of $AH^{\bullet+}$; the latter was measured as a function of the pK_a of a series of pyridine bases. Investigation of the reduction of A^+ by the same techniques led to the determination of the standard potential of the $A^+/A^\bullet$ couple and of the dimerization rate constant of $A^\bullet$. The oxidation of AH as well as the reduction of A^+ are kinetically controlled by follow-up homogeneous chemical steps rather than by the initial electron transfer, which appears as quite fast in both cases. The combination of an ultraslow spectrometric technique with the ultrafast electrochemical techniques allowed the determination of the pK_a of the $AH^{\bullet+}/A^\bullet$ couple from that of the standard potential of the overall reaction $AH \rightleftharpoons A^+ + 2e^- + H^+$ and hence the construction of a Brønsted plot with a known driving force origin for the deprotonation of $AH^{\bullet+}$.

The mechanism of the conversion of NADH to NAD$^+$ and of the reverse reaction, in the coenzyme itself as well as in synthetic analogues, has been the object of considerable experimental work and discussion during the last 15 years.[2] The issue of whether

0002-7863/90/1512-1337$02.50/0

the conversion involves a one-step hydride transfer or a stepwise electron–proton–electron transfer as a function of the opposed reactant has attracted particular attention.[2] In this context, electrochemical oxidation of NADH and reduction of NAD^+ as well as of synthetic analogues[3] would seem an ideally suited approach to the electron–proton–electron transfer mechanism since electrodes are generally considered to abstract or to provide electrons in a stepwise manner. Previous studies,[2c,4,5] however, showed that these expectations are not straightforwardly achieved owing to adsorption of the reactants onto the electrode surface, to possible involvement of superficial oxides in hydride abstraction from AH, and also to the rapidity of the chemical reactions, deprotonation of the $AH^{\bullet+}$ cation radical and dimerization of the $A^\bullet$ radical, coupled with the electron-transfer steps. The latter factor prevented full analysis of the oxidation and reduction mechanisms as well as thermodynamic and kinetic characterization in most cases of interest. Dimerization of $A^\bullet$ could be slowed down considerably by appropriate substitution of the ring carbons.[5j,m,o,w] but it is noteworthy that all true NADH analogues, i.e., having at least one hydrogen on the carbon in the 4-position to the nitrogen, exhibit chemically irreversible oxidative electrochemistry, thus not allowing the intermediates to be characterized within the time scales investigated so far. This is in particular the case with the 10-methylacridan/10-methylacridinium couple:

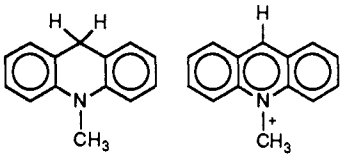

AH A^+

the investigation of which was the object of the work reported hereafter. 10-Methylacridinium ion was also observed to exhibit a completely irreversible cyclic voltammetric reduction wave in acetonitrile up to 5 $V \cdot s^{-1}$.[2c,5w,6] By means of fast cyclic voltammetry and potential step techniques allowed by the used of ultramicroelectrodes, we found it possible to outrun the rapid homogeneous reactions coupled with electron transfer, namely, deprotonation of $AH^{\bullet+}$ and dimerization of $A^\bullet$. This allowed the oxidation and reduction mechanisms to be established as well as the rate constants of the deprotonation of $AH^{\bullet+}$ and of the dimerization of $A^\bullet$, and the standard potentials of the $AH^{\bullet+}/AH$ and $A^+/A^\bullet$ couples to be determined. At this point, the only lacking factor for a full characterization of the oxidation and reduction reaction to be achieved was the pK_a of the $AH^{\bullet+}$ cation radical. This was derived from the standard potential of the overall reaction:

$$A^+ + 2e^- + H^+ \rightleftharpoons AH$$

itself determined by selecting a quinone/hydroquinone couple of known potential and investigation of the oxidation of AH by the quinone and the reduction of A^+ by the hydroquinone. As regards the kinetic aspects, particular emphasis was laid on the deprotonation of the $AH^{\bullet+}$ cation radical. The rate constants were determined for a series of pyridines and correlated with their pK_as.

Table I. Summary of the Thermodynamic and Kinetic Data[a]

standard potentials (in V vs SCE)
$E^\circ_{A^+/AH} = 0.218 - 0.029$ pH (±0.025)
$E^\circ_{AH^{\bullet+}/AH} = 0.860$ (±0.010)
$E^\circ_{A^+/A^\bullet} = -0.460$ (±0.010)
pK_a of the $AH^{\bullet+}/A^\bullet$ couple, 0.6 (±1.2)
standard rate constant of electron transfer (in $cm \cdot s^{-1}$)
$AH^{\bullet+}/AH$, 3.2 (±0.5)
$A^+/A^\bullet$, 3.0 (±0.5)
$A^\bullet$ dimerization rate constant, 3 (±1) × 10^7 $M^{-1} \cdot s^{-1}$

pyridines	pK_a[b]	log k_2[c,d]
Rate Constant of Deprotonation of $AH^{\bullet+}$ by Pyridines		
2-fluoro	4.2	3.3 ± 0.2[e,g]
2-chloro	6.3	4.2 ± 0.1[f]
3-cyano	7.0	4.4 ± 0.1[f]
4-cyano	8.0	4.8 ± 0.1[f]
3-chloro	9.0	5.2 ± 0.2[f,g]
3-fluoro	9.4	5.3 ± 0.2[g]
unsubstituted	12.3	6.5 ± 0.2[g]
3-methyl	13.5	6.3 ± 0.2[g]
3,5-dimethyl	14.5	6.4 ± 0.2[g]
2,4,6-trimethyl	16.8	6.4 ± 0.2[g]

[a] In acetonitrile + 0.6 M NEt_4BF_4, temperature, 20 °C. [b] pK_a in acetonitrile from ref 12. [c] k_2 in $M^{-1} \cdot s^{-1}$. [d] Determined by use of an ultramicroelectrode (5- or 17-μm diameter) unless otherwise stated. [e] Determined by use of a 2 mm diameter gold electrode. [f] Determined by double potential step chronoamperometry. [g] Determined by linear sweep voltammetry.

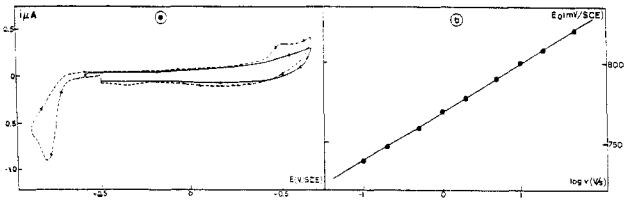

Figure 1. Oxidation of 10-methylacridan (0.9 mM) at a gold 2 mm diameter disk electrode in acetonitrile + 0.6 M NEt_4BF_4 + 10 mM pyridine at 20 °C. (a) Cyclic voltammetry at 0.1 $V \cdot s^{-1}$. (b) Variation of the anodic peak potential (V vs SCE) with the scan rate (v in $V \cdot s^{-1}$) in the range 0.1–100.

Results

Oxidation of 10-methylacridan and reduction of 10-methylacridinium ion were found to exhibit the same cyclic voltammetry and potential step chronoamperometry behaviors whether the working electrode material was platinum or gold. It follows that

(1) (a) Université de Paris 7. (b) Université de Paris 5.

(2) (a) See: References 2b–e and references cited therein. (b) Carlson, B. N.; Miller, L. L. *J. Am. Chem. Soc.* **1985**, *107*, 479. (c) Fukusumi, S.; Koumitsu, S.; Hironaka, K.; Tanaka, T. *J. Am. Chem. Soc.* **1987**, *109*, 305. (d) Kreevoy, M. M.; Ostovic, D.; Lee, I. S.; Blinder, D. A.; King, G. W. *J. Am. Chem. Soc.* **1988**, *110*, 524. (e) Miller, L. L.; Valentine, J. R. *J. Am. Chem. Soc.* **1988**, *110*, 3982. (f) Lee, L. H.; Ostovic, D.; Kreevoy, M. M. *J. Am. Chem. Soc.* **1988**, *110*, 3989.

(3) In the following. NADH and NAD^+, and their synthetic analogues, are designated by the more general notation AH and A^+.

(4) Reviews: (a) Underwood, A. L.; Burnett, R. W. *Electrochemistry of Biological Compounds in Electroanalytical Chemistry*; Bard, A. J., Ed.; Marcel Dekker: New York, 1973; Vol. 6, p 1. (b) Elving, P. J.; Schmakel, C. O.; Santhanam, K. S. V. *CRC Crit. Rev. Anal. Chem.* **1973**, *6*, 1. (c) Dryhurst, G. *Electrochemistry of Biological Molecules*; Academic Press: New York, 1977: pp 524–570.

(5) (a) Klima, J.; Kurfurst, A.; Kutthan, J.; Volke, J. *Tetrahedron Lett.* **1977**, *31*, 2725. (b) Skala, V.; Volke, J.; Ohanka, V.; Kuthan, J. *Collect. Czech. Chem. Commun.* **1977**, *47*, 212. (c) Mahbook, M.; Sheikh, S. U.; Iqbal, M.; Ahmed, R.; Razak, M.; Khan, A. Y. *J. Electroanal. Chem.* **1978**, *89*, 431. (d) Moiroux, J.; Elving, P. J. *J. Am. Chem. Soc.* **1980**, *102*, 6533. (e) Bresnahan, W. T.; Moiroux, J.; Samec, Z.; Elving, P. J. *J. Electroanal. Chem.* **1980**, *116*, 125. (f) Bresnahan, W. T.; Elving, P. J. *J. Am. Chem. Soc.* **1981**, *103*, 2379. (g) Abou-Elenien, G. G.; Rieser, J.; Ismail, N.; Wallenfels, K. *Z. Naturforsch.* **1981**, *36B*, 386. (h) Kitani, A.; Miller, L. L. *J. Am. Chem. Soc.* **1981**, *103*, 3595. (i) Pragst, F.; Kaltofen, B.; Volke, J.; Kuthan, J. *J. Electroanal. Chem.* **1981**, *119*, 301. (j) Hermolin, J.; Levin, M.; Ikagami, Y.; Sawayanagi, M.; Kosower, E. M. *J. Am. Chem. Soc.* **1988**, *103*, 4795. (k) Hermolin, M.; Levin, M.; Kosower, F. M. *Ibid.* 4801. (l) *Ibid.* 4808. (m) Hermolin, J.; Kosower, E. M. *Ibid.* 4813. (n) Trazza, A.; Andruzzi, R.; Carelli, J. *Electrochim. Acta* **1982**, *27*, 347. (o) Kosower, E. M. *Top. Curr. Chem.* **1983**, *112*, 117. (p) Ludvik, J.; Klima, J.; Volke, J.; Kurfurst, A.; Kuthan, J. *J. Electroanal. Chem.* **1983**, *132*, 131. (q) Pavlikova-Raclova, M.; Kuthan, J. *Collect. Czech. Chem. Commun.* **1983**, *48*, 1408. (r) Fukuzumi, S.; Hironaka, K.; Nishizawa, N.; Tanaka, T. *Bull. Chem. Soc. Jpn.* **1983**, *56*, 2220. (s) Blankespoor, R. L.; Miller, L. L. *J. Electroanal. Chem.* **1984**, *171*, 331. (t) Klima, J.; Ludvik, J.; Krikava, M.; Volke, J.; Skala, V.; Kuthan, J. *J. Electroanal. Chem.* **1984**, *161*, 205. (u) Moiroux, J.; Deycard, S.; Malinski, T. *J. Electroanal. Chem.* **1985**, *194*, 99. (v) Ludvik, J.; Turecek, F.; Volke, J. *J. Electroanal. Chem.* **1985**, *188*, 105. (w) Koper, N. W.; Jonker, S. A.; Verhoeven, J. W.; Van Dijk, C. *Recl. Trav. Chim. Pays-Bas*, **1985**, *104*, 296. (x) Ludvik, J.; Volke, J.; Klima *Electrochim. Acta* **1987**, *32*, 1063. (y) Studnickova, M.; Paulova-Klukanova, H.; Turanek, J.; Kovar, J. *J. Electroanal. Chem.* **1988**, *252*, 383.

(6) Whereas in the case of 9-phenyl-10-methylacridinium, the $A^\bullet$ radical is stable for days in the absence of oxygen.[5a]

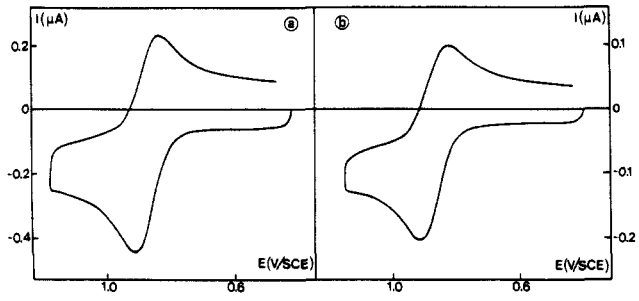

Figure 2. Oxidative cyclic voltammetry of 10-methylacridan (10 mM) in acetonitrile + 0.6 M NEt_4BF_4 (temperature, 20 °C) at a 20 μm diameter platinum (a) and a 17 μm diameter gold (b) disk at 2900 $V \cdot s^{-1}$.

the two reactions can be considered as involving outer-sphere heterogeneous steps associated with homogeneous chemical steps.

Oxidation of 10-Methylacridan. In the absence or in the presence of pyridine or of a substituted pyridine (the pyridines we investigated are listed in Table I), slow-scan (scan rate, v, ranging from 0.1 to 100 $V \cdot s^{-1}$) cyclic voltammograms exhibit a two-electron irreversible anodic wave and one-electron irreversible cathodic wave upon scan reversal (Figure 1a). The latter is the same as the cathodic wave obtained for the reduction of 10-methylacridinium ion as checked with a sample of the iodide salt. The peak potential of the anodic wave varies linearly with log v (Figure 1b) with a 30 mV per log unit slope and appears as independent from the concentration. The peak width, $E_{p/2} - E_p$, does not vary appreciably with the scan rate and has a value of 50 mV. This behavior points to the occurrence of an ECE–DISP1 mechanism:[7]

$$AH - e^- \rightleftharpoons AH^{\bullet+} \quad (1)$$

$$AH^{\bullet+} + B \underset{k_{-2}}{\overset{k_2}{\rightleftharpoons}} A^\bullet + BH^+ \quad (2)$$

$$\text{(ECE)} \qquad A^\bullet - e^- \rightleftharpoons A^+ \quad (3)$$

$$\text{(DISP)} \qquad A^\bullet + AH^{\bullet+} \xrightarrow{k_4} A^+ + AH \quad (4)$$

consisting in a one-electron transfer followed by the deprotonation of the resulting cation radical leading to the neutral radical, which is then immediately oxidized at the electrode surface (ECE) and/or homogeneously by $AH^{\bullet+}$ (DISP). It also shows that, in the framework of such a reaction scheme, the rate-determining step would be the deprotonation reaction rather than the initial heterogeneous electron transfer or the second electron transfer.

The anodic wave becomes reversible, with a one electron per molecule stoichiometry, upon raising the scan rate up to values ranging from 1000 to 100 000 $V \cdot s^{-1}$ according to the nature and concentration of the base present in the medium. Figure 2 shows a typical example of cyclic voltammograms obtained under such conditions in the case where no base was added to the solution. The standard potential of the $AH/AH^{\bullet+}$ redox couple can be immediately derived from such experiments as the midpoint between the anodic and cathodic peak potentials. A value of 0.860 V vs SCE (±10 mV) was thus found. The value of the standard electron-transfer rate constant, k_s, was derived from the voltammograms obtained at scan rates between 10 000 and 80 000 $V \cdot s^{-1}$ by the same simulation procedure as described earlier[8] assuming that $\alpha = 0.5$ and taking $D = 10^{-5}$ $cm^2 \cdot s^{-1}$. We thus found $k_s = 3.2 \pm 0.5$ $cm \cdot s^{-1}$.

The transition between the two-electron irreversible behavior observed at low scan rates and the one-electron reversible behavior at high scan rates was used to derive the rate constant of $AH^{\bullet+}$ deprotonation in the presence of various pyridine bases, B (Table I). To simplify the kinetic analysis, $AH^{\bullet+}$ deprotonation was forced to take place under pseudo-first-order conditions by adding the base in at least 10-fold excess over the AH concentration. With the weakest bases, namely, for those having a pK_a below 9, the medium was buffered by introduction of different amounts of the conjugated acid to ensure that the deprotonation involves the added pyridine bases and not the solvent itself or adventitious basic impurities such as residual water or amines present in the tetraalkylammonium supporting electrolyte. The addition of BH^+ was found not to affect the overall kinetics for pyridines of higher pK_a and was thus not necessary to obtain the deprotonation rate constant.

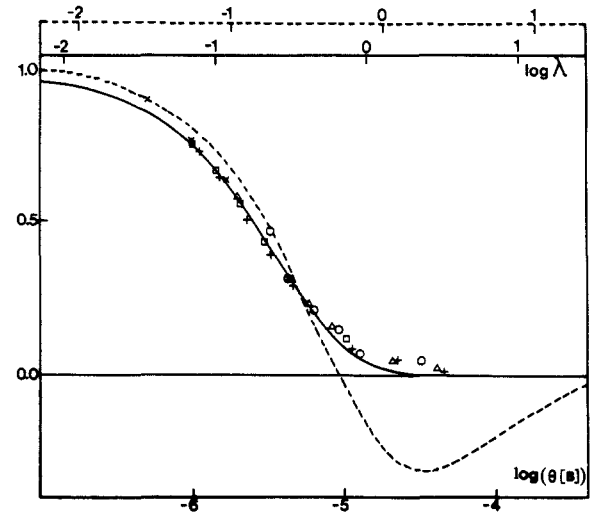

Figure 3. Electrochemical oxidation of 10-methylacridan (5 mM) in acetonitrile + 0.6 M NEt_4BF_4 (temperature 20 °C) in the presence of 4-cyanopyridine, B, and of the conjugated acid BH^+. Double potential step chronoamperometry from 0.6 to 1.0 V vs SCE and back at a 5 μm diameter (x) and a 17 μm diameter (+, ○, △, □) gold disk microelectrode. Variation of the current ratio R (see text) with the inversion time θ, and with the concentration of B and BH^+. +: [B] = 45 mM, $[BH^+]$ = 45 mM. ○: [B] = 124 mM, $[BH^+]$ = 42 mM. △: [B] = 83 mM, $[BH^+]$ = 84 mM. (□, ×): [B] = 41 mM, $[BH^+]$ = 126 mM. The solid line represents the theoretical variation of R with the dimensionless rate parameter $\lambda = (k_2[B]\theta)$ (k_2 forward rate constant of reaction 2) for a DISP1 mechanism and the dotted line, the variation with the same parameter λ for an ECE mechanism.

Double-potential step chronoamperometry (DPSC)[7b,9a] with an ultramicroelectrode[9b] was used with the four least basic pyridines. The potential is stepped sufficiently beyond the oxidation potential of AH for the current to be unaffected by ohmic drop and by the kinetics of the initial electron-transfer step. At a time θ, which can be varied from one experiment to the other, the potential is stepped back to its initial value. The anodic current is measured at time θ,$i(\theta)$, and the cathodic current at time 2θ,$i(2\theta)$. The ratio $i(2\theta)/i(\theta)$ is normalized toward the value it would have in the absence of follow-up chemical steps so as to obtain the ratio

$$R = [i(2\theta)/i(\theta)]/[i(2\theta)/i(\theta)]_{diff}$$

which thus varies from 1 to 0 as the deprotonation reaction gets faster and faster as compared to the diffusion rate. The latter increases as θ decreases. On the other hand, the rate of the chemical step is expected to increase with the concentration of base introduced in the solution. Figure 3 summarizes a typical set of DPSC experiments in which the ratio R was measured for several values of θ and of concentration of base. In this case, as well as in the three others, the experimental points fit the theoretical variations expected for a DISP1 mechanism and do not fit those expected for an ECE mechanism (Figure 3).[10] Fitting

(7) (a) Nadjo, L.; Savéant, J.-M. *J. Electroanal. Chem.* **1973**, *48*, 113. (b) Amatore, C.; Gareil, M.; Savéant, J.-M. *J. Electroanal. Chem.* **1983**, *147*, 1.

(8) (a) Andrieux, C. P.; Garreau, D.; Hapiot, P.; Pinson, J.; Savéant, J.-M. *J. Electroanal. Chem.* **1988**, *243*, 321. (b) Andrieux, C. P. Garreau, D.; Hapiot, P.; Savéant, J.-M. *J. Electroanal. Chem.* **1988**, *248*, 447. (c) Andrieux, C. P.; Hapiot, P.; Savéant, J.-M. *J. Phys. Chem.* **1988**, *92*, 5987.

(9) (a) Andrieux, C. P.; Savéant, J.-M.; Electrochemical Reactions. In *Investigations of Rates and Mechanisms of Reactions*; Bernasconi, C. F., Ed.; Wiley: New York, 1986; Vol. 6, 4/E, Part 2, pp 305–390. (b) Andrieux, C. P.; Hapiot, P.; Savéant, J.-M. *J. Phys. Chem.* **1988**, *92*, 5992.

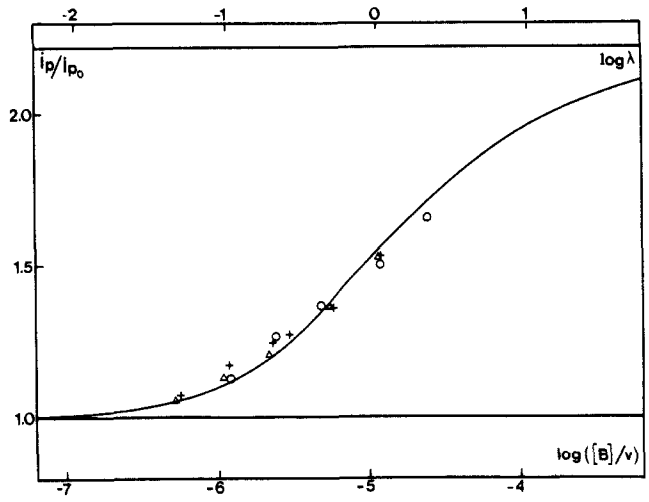

Figure 4. Electrochemical oxidation of 10-methylacridan (2 mM) in acetonitrile + 0.6 M $NEt4BF_4$ (temperature, 20 °C) in the presence of pyridine, B, and of the conjugated acid BH^+. Variations of the linear sweep voltammetry peak current ratio i_p/i_{p_0} (i_p/i_{p_0}, peak currents in the presence and in the absence of pyridine, respectively) with the scan rate (from 2000 to 40 000 $V \cdot s^{-1}$) and the concentration of pyridine at a 5-μm gold microelectrode. O: [B] = 40 mM, $[BH^+]$ = 0. +: [B] = 20 mM, $[BH^+]$ = 0. Δ: [B] = 19 mM, $[BH^+]$ = 21 mM. The solid line represents the theoretical variations of i_p/i_{p_0} with the dimensionless parameter $\lambda = (k_2[B]/v)(RT/F)$.

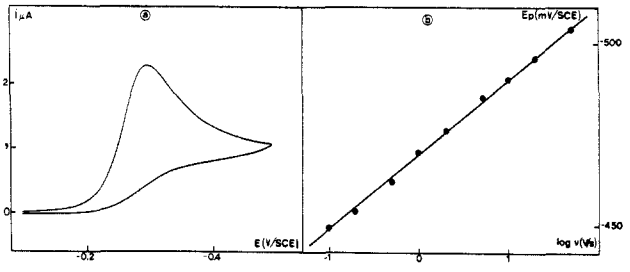

Figure 5. Reduction of 10-methylacridinium iodide in acetonitrile +0.6 NEt_4BF_4 at a 2-mm platinum electrode (temperature, 20 °C). (a) Cyclic voltammogram at 0.1 $V \cdot s^{-1}$ for a 1.09 mM concentration. (b) Variation of the peak potential with scan rate for a 0.9 mM concentration.

of the experimental points with the DISP1 working curve thus allows the determination of k_2. The values thus found with the four weakest bases are listed in Table I.

For all the remaining pyridines, we employed linear sweep voltammetry,[9a] again with an ultramicroelectrode,[11] taking advantage of the fact that the peak height passes, in a known manner,[7b,8c,9a] from a two electron per molecule to one electron per molecule stoichiometry as the scan rate is raised in the framework of an ECE or a DISP1 mechanism. It was again found that a DISP1 mechanism rather than an ECE mechanism takes place. Fitting of the experimental points with the DISP1 working curve[7b] (Figure 4) thus allows the determination of k_2. The ensuing values are listed in Table I. Both DPSC and linear sweep voltammetry were used in the case of 3-chloropyridine, leading to the same result.

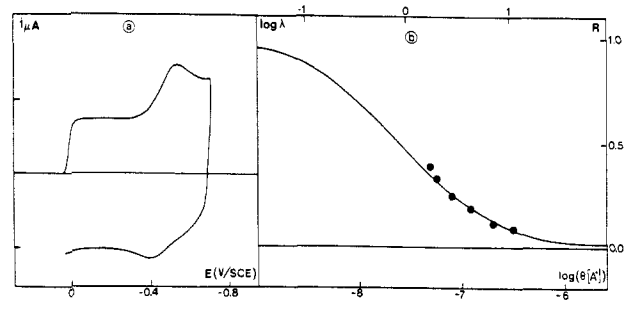

Figure 6. Reduction of 10-methylacridinium (2 mM) in acetonitrile + 0.6 M NEt_4BF_4 (temperature, 20 °C). (a) Cyclic voltammetry at a 5 μm diameter gold disk electrode. Scan rate, 15 000 $V \cdot s^{-1}$. (b) Variation of the DPSC current ratio $R = [i(2\theta)/i(\theta)]/[i(2\theta)/i(\theta)]_{diff}$ with the inversion time θ at a 10-μm platinum electrode disk electrode stepping from −0.2 to −0.7 V vs SCE and back. Solid line: working curve for the mechanism $A^+ + e^- \rightleftharpoons A^\bullet$, $2A^\bullet \rightarrow$ dimer. ($\lambda = k_6[A^+]\theta$).

Reduction of the 10-Methylacridinium Ion. Figure 5a shows a typical cyclic voltammogram of A^+ at low scan rate. A one-electron irreversible wave is observed from 0.1 to 100 $V \cdot s^{-1}$. The peak potential varies linearly with the logarithm of the scan rate (Figure 5b) with a slope of −20 mV per unit. It also varies with the bulk concentration of A^+ by 20 mV per 10-fold increase. The peak width is independent of both scan rate and concentration, with a value of 39 mV. These observations indicate that the reduction mechanism involves a fast electron transfer followed by the irreversible dimerization of the $A^\bullet$ radicals thus generated:[9a,13a]

$$A^+ + e^- \rightleftharpoons A^\bullet \quad (5)$$

$$2A^\bullet \xrightarrow{k_6} \text{dimer} \quad (6)$$

Upon raising the scan rate, the cyclic voltammogram tends to become reversible. Full reversibility is reached, using an ultramicroelectrode at 15 000 $V \cdot s^{-1}$ for a 2 mM concentration (Figure 6a). The standard potential of the $A^+/A^\bullet$ couple is thus found equal to −0.460 V vs SCE as the midpoint between the cathodic and anodic peak potentials. The standard rate constant was found equal to 3 (±0.5) $cm \cdot s^{-1}$ by using the same procedure as described above. The dimerization rate constant was determined by using again an ultramicroelectrode for double potential step chronoamperometry.[9b] A value of 3 (±1) × 10^7 $M^{-1} \cdot s^{-1}$ was thus found by fitting the experimental points with the appropriate working curve (Figure 6b).[13b]

In an attempt to determine the rate constant of the protonation of the $A^\bullet$ radical, k_{-2}, the experiments described in Figure 5 were repeated in the presence of equimolar mixtures of 2-fluoropyridine and of the corresponding protonated pyridinium. Under such conditions, there is the possibility of a competition between the dimerization reaction (6) and the protonation of $A^\bullet$ (2). If the latter occurs, the resulting $AH^{\bullet+}$ radical would be immediately reduced by $A^\bullet$ (reaction 4) at a rate close to the diffusion limit as discussed earlier. This would result in a DISP1 rather than in a DISP2 process since $k_4[A^+] \gg k_2[B]$. On the other hand, an ECE pathway would not be able to compete with the DISP1 since k_{-2} is very small,[7b] as discussed below. An easy measure of the competition between this DISP1 process, governed by the

(10) In this analysis, we neglected, for the following reasons, the possible occurrence of another DISP mechanism, "DISP2", in which the rate-determining step would be reaction 4, with reaction 2 acting as a preequilibrium.[7b,9a] The DISP2 mechanism would interfere if $k_4[AH] \ll k_2[BH^+]$, whereas the DISP1 mechanism would prevail in the opposite case. From the value of the standard potential of the $AH^{\bullet+}/AH$ couple already determined and from that of the $A^+/A^\bullet$ couple that will be determined in the following, the driving force of the reaction 4 is of the order of 1.2 eV. Since the intrinsic barriers for both the $AH^{\bullet+}/AH$ and $A^+/A^\bullet$ couples are small as result from the high values found for the standard heterogeneous electron-transfer rate constants, it follows that reaction 4 is likely to be at the diffusion limit, i.e., 10^{10} $M^{-1} \cdot s^{-1}$. $k_4[AH]$ is thus of the order of 10^7 s^{-1}. On the other hand, as apparent in the following, k_{-2} is quite small, namely, of the order of 2 × 10^3 $M^{-1} \cdot s^{-1}$. The condition $k_4[AH] \ll k_2[BH^+]$ is thus largely fulfilled in all experimental conditions dealt with in the present work.

(11) (a) Howell, J. O.; Wightman, R. M. *Anal. Chem.* **1984**, *56*, 524. (b) Wehmeyer, K. R.; Wightman, R. M. *Anal. Chem.* **1985**, *57*, 1989. (c) Howell, J. O.; Kuhr, W. G.; Ensman, R. E.; Wightman, R. M. *J. Electroanal. Chem.* **1986**, *209*, 77. (d) Montenegro, M. I.; Pletcher, D. *J. Electroanal. Chem.* **1986**, *200*, 371. (e) Ficht, A.; Evans, D. H. *J. Electroanal. Chem.* **1986**, *202*, 83. (f) Amatore, C.; Jutand, A.; Pflüger, F. *J. Electroanal. Chem.* **1987**, *218*, 361. (g) Wipf, D. O.; Kristensen, E. W.; Deakin, M. R.; Wightman, R. M. *Anal. Chem.* **1988**, *60*, 306.

(12) (a) Cauquis, G.; Deronzier, A.; Serve, D.; Vieil, E. *J. Electroanal. Chem.* **1975**, *60*, 205. (b) Schlesener, C. J.; Amatore, C.; Kochi, J. K. *J. Am. Chem. Soc.* **1984**, *106*, 7472.

(13) (a) Savéant, J.-M.; Vianello, E. *C.R. Acad. Sci. Paris* **1963**, *256*, 2597. (b) Amatore, C.; Garreau, D.; Hammi, M.; Pinson, J.; Savéant, J.-M. *J. Electroanal. Chem.* **1985**, *184*, 1.

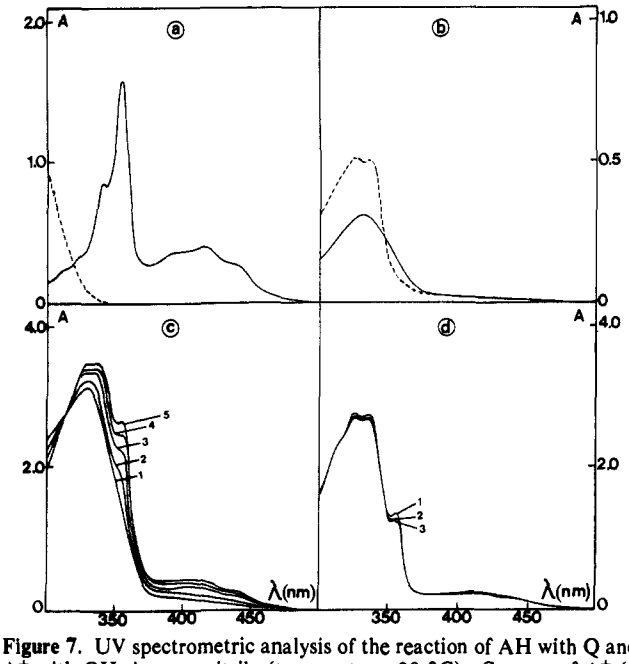

Figure 7. UV spectrometric analysis of the reaction of AH with Q and A^+ with QH_2 in acetonitrile (temperature, 20 °C). Spectra of A^+ (1 mM) (—) and AH (1 mM) (---) (a) and of Q (1 mM) (—) and QH_2 (1 mM) (---) (b). (c) Reaction of 0.01 M AH with 0.1 M Q in a 0.05 M pyridinium buffer. Spectra of aliquots diluted 20 times as a function of time: (0 h), 2 (14 h), 3 (38 h), 4 (62 h), 5 (86 h). (d) Reaction of 0.01 M A^+ with 0.1 M QH_2 in a 0.01 M collidine/0.001 M collidinium buffer. Spectra of aliquots diluted 20 times as a function of time: 1 (0 h), 2 (32 h), 3 (56 h).

protonation reaction and the dimerization of A•, is the value of the current ratio i_p/i_p^d (i_p, observed peak current; i_p^d, peak current that could correspond to a predominating dimerization process at the same scan rate). As shown elsewhere,[14] i_p/i_p^d is a known function of the dimensionless parameter $(k_6[A^+]/(k_{-2}[B])^{3/2})\cdot(Fv/RT)^{1/2}$. For example $i_p/i_p^d = 1.05$ when the parameter is equal to 6.3×10^2. We found experimentally that addition of the 2-fluoropyridine buffer up to 10 mM did not produce any noticeable increase of the peak height. Assuming that the peak currents are measured with a 5% accuracy, it follows than the parameter is larger than 6.3×10^2 and thus that $k_{-2} > 2.10^{-3}$ $M^{-1}\cdot s^{-1}$. Since we know k_2, we can conclude that the pK_a of the $AH^{\bullet+}/A^\bullet$ couple is smaller than 4.2.

Determination of the A^+/AH Standard Potential. A more precise estimation of the pK_a of the $(AH^{\bullet+}/A^\bullet)$ acid–base couple was obtained from the determination of the standard potential, $E^\circ_{A^+/AH}$ of the overall reaction:

$$A^+ + 2e^- + H^+ \rightleftharpoons AH$$

For this, we opposed the A^+/AH couple to a quinone/hydroquinone couple, namely, 1,4-naphthaquinone/1,4-dihydroxynaphthalene (Q/QH_2), the standard potential of which can be determined by electrochemical means:

$$Q + AH + H^+ \rightleftharpoons QH_2 + A^+ \qquad (7)$$

A pyridine/pyridinium or collidine (2,4,6-trimethylpyridine)/collidinium buffer was used to maintain the pH. The reaction is extremely slow in both directions. The establishment of equilibrium would thus require a long period of time during which chemical transformations of A^+, Q, and QH_2 would take place, thus preventing a sound determination of the equilibrium constant. This was rather derived from the forward and backward rate constants, themselves determined by reacting separately Q with AH and QH_2 with A^+ without attempting to reach equilibrium in each case. The kinetics of both reactions were followed by monitoring the variation of the absorbance with time at 356 nm, a wavelength at which the molar absorbance of A^+ is much larger than those of all other intervening species (see Figure 7a and b). For the oxidation of AH by Q, the initial composition of the solution was [AH] = 0.01 M, [Q] = 0.1 M, the buffer being either a pyridine/pyridinium mixture (0.05 M/0.05 M, pH = 12.3)[12,15] or a collidine/collidinium mixture (0.05 M/0.05 M, pH = 16.8).[12,15] Figure 7c shows the variation of the UV spectrum during a period of time extending up to 86 h. The spectra of pure solutions of AH, A^+, QH_2, and Q are represented in Figure 7a and b. We checked that, in the two buffers, none of the four reactants taken separately undergoes any noticeable decomposition during this period of time. The absorbances of AH and QH_2 at 356 nm are negligible throughout the experiment. That of Q, although not negligible, remains constant owing to its large excess over AH. The ratio $(A_0 - A_t)/(A_0 - A_\infty)$ (A_0, A_t, absorbance at time 0 and t; A_∞, absorbance that would have been observed upon total conversion of AH into A^+ is easily calculated from the spectra of pure samples of A^+, Q, and QH_2) is thus a measure of the fraction of AH that has been converted into A^+ at time t. At both pHs, the ln $[(A_0 - A_t)/(A_0 - A_\infty)]$ vs time plots were found to be linear, indicating that the reaction is first order in A^+ and that the backward reaction can be neglected. The slopes of these plots were practically the same at pH 12.3 and 16.9, leading to a value of the forward rate constant $k_f = 0.16 \pm 0.01$ $M^{-1}\cdot h^{-1}$. The lack of dependence of k_f upon pH indicates that the first of the following steps is rate determining (CH^+/C designates the buffer couple):

$$Q + AH \rightleftharpoons A^+ + QH^-$$

$$QH^- + CH^+ \rightleftharpoons QH_2 + C$$

The initial conditions for the reduction of A^+ by QH_2 were $[A^+]$ = 0.01 M, $[QH_2]$ = 0.1 M, [C] = 0.01 M, $[CH^+]$ = 0.001 M (C, collidine; CH^+, collidinium). The composition of the buffer was selected so as to be as basic as possible for having the fastest reaction compatible with the stability of the various reactants during the time of the experiment. The latter condition was fulfilled for a time period of 56 h. The variation of the absorbance during this period of time was rather small, as shown Figure 7d, x being the fraction of A^+ converted into AH at time t ($x = (A_0 - A_t)/(A_0 - A_\infty)$, with the same definition of the absorbances as above), the kinetics of the reaction are described by

$$\frac{dx}{dt} = \frac{kK_Q}{K_C}\frac{(1-x)^2}{1+10x} - 0.01k_fx^2$$

corresponding to the two-step reaction

$$QH_2 + C \rightleftharpoons QH^- + CH^+$$

$$QH^- + A^+ \underset{k_f}{\overset{k}{\rightleftharpoons}} Q + AH$$

where the first step functions as a preequilibrium vis-à-vis the second rate-determining step (K_Q and K_C are the dissociation equilibrium constants of QH_2 and CH^+, respectively). The iterative numerical resolution of the above equation led to

$$kK_Q/K_C = 4.5\ (\pm 1.4) \times 10^{-3}\ M^{-1}\cdot h^{-1}$$

k_b, the rate constant of backward reaction 5, is then obtained as

$$k_b = kK_Q/[H^+]$$

Thus,[16] (in $M^{-1}\cdot h^{-1}$)

$$\log k_b = -19.15\ (\pm 0.1) + pH$$

$E^\circ_{AH^+/AH}$ is thus related to E°_{Q/QH_2} (at 20 °C) by

$$E^\circ_{AH^+/AH} = E^\circ_{Q/QH_2} - 0.029 \log (k_f/k_b)$$

(14) Hapiot, P.; Savéant, J.-M. *J. Electroanal. Chem.*, to be published.

(15) (a) Neglecting homoconjugation by assuming that the homoconjugation constant is of the same order of magnitude as for pyridine.[15b] (b) Coetze, J. F. Ionic Reactions in Acetonitrile. *Prog. Phys. Org. Chem.* **1967**, *4*, 77.

(16) (a) $pK_a = 27.2$ and homoconjugation constant = 1.1×10^2 M^{-1}.[16c] (b) $pK_a = 27.3$ and homoconjugation constant = 4.7×10^3 M^{-1}.[16c] (c) Kolthoff, I. M.; Chantooni, M. K.; Bhowmik, S. *J. Am. Chem. Soc.* **1968**, *90*, 23.

i.e. (in V)

$$E^\circ_{A^+/AH} = E^\circ_{Q/QH_2} - 0.029\ pH + 0.532\ (\pm 0.005)$$

E°_{Q/QH_2} was determined as described in the Experimental Section:

$$E^\circ_{Q/QH_2} = -0.750 - 0.058\ pH\ (\pm 0.020)\ V\ vs\ SCE$$

it follows that, at 20 °C

$$E^\circ_{A^+/AH} = 0.218 - 0.029\ pH\ (\pm 0.025)\ V\ vs\ SCE$$

From this value and those of $E^\circ_{AH^{\bullet+}/AH}$ and $E^\circ_{A^+/A^\bullet}$ previously determined, the pK_a of the $AH^{\bullet+}/A$ couple can be estimated:

$$0.058\ pK_a = 2E^\circ_{A^+/AH} - E^\circ_{AH^{\bullet+}/AH} - E^\circ_{A^+/A^\bullet}$$

as

$$pK_a = 0.6\ (\pm 1.2)$$

Discussion

Combination of ultrafast and ultraslow kinetic techniques allowed a detailed mechanistic, kinetic, and thermodynamic analysis of the oxidation of 10-methylacridan and the reduction of 10-methylacridinium, which can be summarized as follows.

The oxidation of AH occurs along an ECE-type mechanism in which the first electron transfer occurring at the electrode is followed by an homogeneous, rate-determining, deprotonation step and then by a second electron transfer taking place in the solution where the $A^\bullet$ radical is oxidized by the parent $AH^{\bullet+}$ radical (i.e., a "DISP1" mechanism). On the other hand, the reduction of A^+ leading to the corresponding dimer consists, after the formation of the $A^\bullet$ radical, in a simple, rate-determining homogeneous radical–radical coupling reaction. In both cases, the rate-determining step is the coupled homogeneous chemical step rather than the initial electron transfer. The latter process is indeed quite fast, having a standard rate constant over 1 $cm \cdot s^{-1}$ in both cases (Table I).

Previous estimations of the standard potentials of the $AH^{\bullet+}/AH$ and $A^+/A^\bullet$ redox couples have been based on the assumption that the initial electron transfer is rate determining in the electrochemical oxidation of AH and reduction of A^+ and that it obeys a quadratic Marcus-type activation–driving force free energy relationship.[2c] The standard potentials and intrinsic barriers of both electron-transfer processes were thus derived from the values of the cyclic voltammetric peak potentials and the variations of the transfer coefficient with the electrode potential at low scan rates. The accuracy of such determination has been questioned in view of the difficulty of measuring small variations of the transfer coefficient in such restricted a range of scan rates, i.e., such restricted a range of driving forces.[2e] There is in fact a more fundamental problem in applying such a procedure to the present reactions, since in both cases, the rate-determining step is not the initial electron-transfer step but a follow-up homogeneous chemical step–deprotonation for the oxidation of AH and radical–radical coupling for the reduction of A^+.[17]

The Brønsted plot relating the deprotonation rate constant of $AH^{\bullet+}$ to the pK_as of the pyridine bases is shown in Figure 8. Unlike most carbon acids investigated so far,[18] and particularly cation radicals,[18c] plateauing of the curve at high driving forces is clearly visible. The other linear portion of the plot has a slope of 0.39, unambiguously indicating that the forward and backward reactions are under activation control. All the experimental points unambiguously belong to the exergonic region of the deprotonation reaction since we know the origin of the driving force scale. The height of the high driving force plateau (log k_2 = 6.2) is much

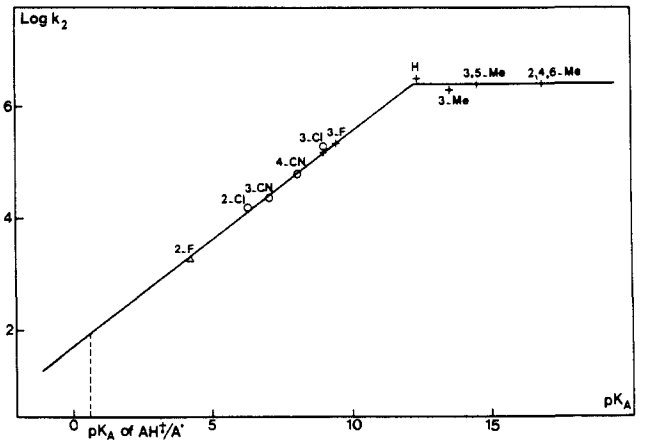

Figure 8. Brønsted plot relating the deprotonation rate constants of $AH^{\bullet+}$ to the pK_as of the pyridine bases in acetonitrile.

below the diffusion limit, pointing to the involvement of a significant work term required for bringing the reactants in an appropriate configuration for proton transfer to occur. The intrinsic barrier (including the work term), as obtained from the extrapolation of the plot to zero driving force, is rather large. It would thus seem that favorable conditions exist for attempting to test theoretical models such as that derived from the extension of Marcus theory to proton transfer.[18,19] In this respect the situation is more favorable than in the many cases where the origin of the driving force scale, the work terms, and the intrinsic barrier must all be derived from Brønsted plots showing subtle variation of the transfer coefficient with the driving force. In our opinion, such attempts should however await further experimental investigations (role of solvent, temperature, structure variation) that could provide a reasonable picture of the origin of the work term.

The value found for the standard potential of the AH/A^+ couple, 0.218–0.029 pH V vs SCE, indicates that the 9-methylacridinium cation is a quite powerful oxidant. This falls in line with a previous approximate estimation of this potential in water at pH 7,[21] which showed that 9-methylacridinium was the strongest oxidant in an extended series of NAD^+ analogues. A quantitative comparison between the two values is, however, difficult since the solvents are different and so are the pH scales.

Among the various thermodynamic constants listed in Table I, the strongest discrepancy with previous results appears for the pK_a of the $AH^{\bullet+}/A^\bullet$ acid–base couple. A previous investigation[2c] based on the Brønsted plot of the rate constants of the reaction of $AH^{\bullet+}$ with various pyridines in acetonitrile led to the conclusion that the pK_a is equal to that of the couple that would have a pK_a of 2 in water, i.e., a pK_a of 8.5 in acetonitrile (see Table IV and Figure 4 in ref 2c and Table I in the present paper). We find the pK_a 8 pH (acetonitrile) units lower (Table I). The source of the discrepancy appears to be the following. In ref 2c, the pK_a was derived from the Brønsted plot of the $AH^{\bullet+}$ deprotonation rate constants, whereas it was determined in a more direct manner in the present work. There are no dramatic differences between the rate constants determined in ref 2c and ours.[20] However, the rate constants were plotted against the pK_a of the pyridine bases in water rather than in acetonitrile. The ensuing narrowing of the pH scale thus led to the conclusion that in the rising linear portion of the plot observed at low pH the backward reaction, i.e., protonation of $A^\bullet$ by the pyridinium, is under diffusion control. On the other hand, the plateau observed at the highest pHs was thought to indicate diffusion control of the forward reaction in

(17) (a) Curiously enough, however, the values thus found for the standard potentials (0.80 V vs SCE for the $AH^{\bullet+}/AH$ couple and −0.43 V vs SCE for the $A^+/A^\bullet$ couple[2c]) are coincidentally close to those obtained in the present work.

(18) (a) Kresge, A. J. *Acc. Chem. Res.* **1975**, *8*, 354. (b) Keefe, J. R.; Kresge, A. J. Catalysis by Small Molecules. In *Homogeneous Solutions in Investigation of Rates and Mechanisms of Reactions*: Techniques of Chemistry; Bernasconi, C. F., Ed.; Wiley Interscience: New York, 1986; Part I, Vol. VI, pp 747–790. (c) Schlesener, C. J.; Amatore, C.; Kochi, J. K. *J. Am. Chem. Soc.* **1984**, *106*, 7472.

(19) (a) Marcus, R. A. *J. Phys. Chem.* **1968**, *72*, 891. (b) Kreevoy, M. M.; Truhlar, D. G. *Transition State Theory in Investigation of Rates and Mechanisms of Reactions*; Techniques of Chemistry; Bernasconi, C. F., Ed.; Wiley-Interscience: New York, 1986; Part I, Vol. VI, pp 13–96.

(20) They agree within 1 order of magnitude. The observed differences may arise from the different composition of the reaction medium (presence of a supporting electrolyte in our case and not in ref 2c).

(21) Ostovic, D.; Lee, I.-S. H.; Roberts, R. M. G.; Kreevoy, M. M. *J. Org. Chem.* **1985**, *50*, 4206.

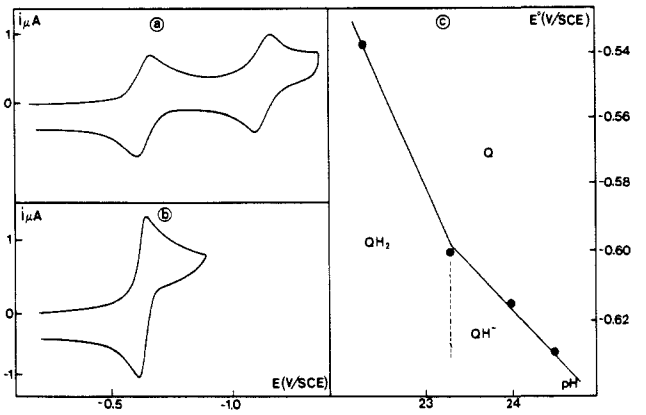

Figure 9. Cyclic voltammetry of 0.2 mM 1,4-naphthoquinone in acetonitrile +0.1 M NEt_4BF_4 at 20 °C at a platinum 2 mm diameter electrode in the absence of acid (a) and in the presence of a 8.8 mM phenol/1.2 mM phenate buffer (b). (c) Potential pH diagram of the 1,4-naphthoquinone/1,4-dihydroxynaphthalene couple.

spite of a plateau value being 3–4 orders of magnitude below the diffusion limit. The pK_a was then determined as the pH corresponding to the intersection of these two linear portions of the plot. In fact, the low pH rising linear section of the plot has a slope (0.39) much smaller than 1, clearly indicating that the forward and backward reactions are under activation control. The intersection between the two linear portions of the plot thus does not correspond to the pK_a of the $AH^{\bullet+}/A^{\bullet}$ couple, but is located, as are all the experimental data points, in a substantially exergonic region of the deprotonation reaction.

Experimental Section

Reagents. All pyridines used were commercially available. 10-Methylacridan and 10-methylacridinium iodide were prepared according to a previously published procedure.[22] The solution were prepared with acetonitrile (Merck Uvasol) and deoxygenated with argon before use. Tetraethylammonium tetrafluoroborate (Fluka, puriss) was used as supporting electrolyte.

Apparatus and Procedures. The ultramicroelectrodes were prepared by sealing gold or platinum wires (Goodfellow Metal Ltd.) according to a previously described procedure.[8a] The reference electrode was an aqueous SCE and the counterelectrode a platinum grid. The cell was placed in a Faraday cage. The potentiostat with a three-electron configuration was the same as previously described.[8,23] Chronoamperograms and voltammograms were recorded with a Nicolet 4094C/4180 (8 bits, 5-ns sampling time) digital oscilloscope. The function generator was an Enertec 4431. In double potential step experiments, the current-time curves were repeated 10 times and accumulated before transfer into an IBM PC-AT microcomputer for treatment.[9b] The whole set of measurements was repeated again 10 times. Under these conditions, the dispersion in the measurement of R was found to be less than 0.05. A 17-μm gold electrode was used for times θ between 24 μs and 1 ms, and a 5-μm gold electrode for time θ between 3 to 50 μs.[9b] In linear sweep voltammetry experiments, each curve was repeated 10 times and accumulated in the digital oscilloscope. The values of i_p (peak in presence of bases) and i_{p_0} (peak current is absence of bases) were measured directly at the same electrode with the same solution, by subtracting the base line.[24] The dispersion error on the value of the ratio i_p/i_{p_0} was found to be less than 0.15. Experimental absorption spectra were obtained with a Varian Superscan 3 UV-visible spectrophotometer. The reactions were carried out at 20 °C under nitrogen atmosphere and the spectra were recorded from aliquots diluted 20 times. $E°_{Q/QH_2}$ was determined as follows. In an 8.8 mM phenol/1.2 mM phenate buffer (pH = 24.5[16a]); Q (0.2 mM) gives rise to a single two-electron reversible cyclic voltammogram (30 mV between cathodic and anodic peaks) at 0.1 $V \cdot s^{-1}$ (Figure 9). The standard potential, measured as the midpoint between the cathodic and anodic peak is then −0.630 V vs SCE. Upon raising the pH the single two-electron wave splits into two waves, whereas upon decreasing the pH it loses its reversibility. Zero-current potentiometric measurements were also carried out in acetic/acetate buffers at pH = 24, 23.3, and 23.3.[16b] At pH 24, an $E°$ value of −0.615 V vs SCE was obtained almost instantaneously, whereas stable values of −0.600 and −0.540 V vs SCE were obtained at pH 23.3 and 22.3 after 10- and 60-min equilibration periods, respectively. The resulting $E°$ − pH plot (Figure 9b) thus shows two regions with 29 and 58 mV slopes corresponding to the $Q/QH^{\bullet-}$ and Q/QH_2 couples, respectively. The value of $E°_{Q/QH_2}$ ensues.[25]

(22) Roberts, R. M. G.; Ostovic, D.; Kreevoy, M. M. *Faraday Discuss. Chem. Soc.* **1982**, *74*, 257.

(23) Garreau, D.; Hapiot, P.; Savéant, J.-M. *J. Electroanal. Chem.* **1989**, *272*, 1.

(24) The effects of ohmic drop, mutual influence of the ohmic drop and capacitive current,[8a] and heterogeneous electron-transfer kinetics[7a] on the ratio i_p/i_{p_0} were checked to be negligible in our working conditions.

(25) And thus the value of the pK_a of the QH_2/QH^- couple is 23.3 (±0.3).

Evidence for Lifetime Distributions in Cyclodextrin Inclusion Complexes

Frank V. Bright,* Gino C. Catena, and Jingfan Huang

Contribution from the Department of Chemistry, Acheson Hall, State University of New York at Buffalo, Buffalo, New York 14214. *Received July 24, 1989*

Abstract: Multifrequency phase and modulation fluorescence spectroscopy are used to study 1:1 inclusion complexes of β-cyclodextrin (βCD) with several anilinonaphthalene sulfonate (ANS) probes. Our time-resolved fluorescence results indicate that the inclusion complex is described most accurately by distributed fluorescence lifetime models. This indicates that the ANS probe is not in a single discrete environment within the cyclodextrin cavity but in an array of cyclodextrin-cavity environments all in equilibrium with one another.

Cyclodextrins (CD's) are toroidally shaped polysaccharides made up of six to eight D-glucose monomers.[1] The CD cavities are hydrophobic and have internal diameters ranging from 4.7–8.3 Å.[2] Because of the size and hydrophobic nature of CD's they form inclusion complexes with many small molecules.[1,2] As a result, CD's have been used extnesively to model protein–ligand and enzyme–substrate interactions,[3] have found widespread ap-

* Author to whom all correspondence should be directed.

(1) See, for example: (a) Baeyens, W. R. G.; Ling, B. L.; De Moerloose, P.; Del Castillo, B.; De Jonge, C. *Ann. Rev. Acad. Farm.* **1988**, *54*, 698. (b) *Inclusion Compounds*; Atwood, J. L., Davis, J. E. D., Mac Nicol, D. D., Eds.; Academic Press: London, 1984; Vol. 2 and 3.

0002-7863/90/1512-1343$02.50/0